To the Graduate Council:

I am submitting herewith a thesis written by Thibor R. R. Bernardon entitled "Testing and Performance Evaluation of the Longitudinally Segmented Forward Hadronic Calorimeter (LFHCAL)." I have examined the final paper copy of this thesis for form and content and recommend that it be accepted in partial fulfillment of the requirements for the degree of Master of Science, with a major in Physics.

Dr. Christine Nattrass, Major Professor

We have read this thesis
and recommend its acceptance:

Dr. Miguel Madurga

Dr. Robert Grzywacz

Accepted for the Council:

Dixie L. Thompson

Vice Provost and Dean of the Graduate School

Testing and Performance Evaluation of the Longitudinally Segmented Forward Hadronic Calorimeter (LFHCAL)

A Thesis Presented for the

Master of Science

Degree

The University of Tennessee, Knoxville

Thibor R. R. Bernardon

May 2025

© by Thibor R. R. Bernardon, 2025
All Rights Reserved.

Para o amor da minha vida, Maria, e o ódio de meus inimigos,

Acknowledgements

I would like to thank Dr. Oskar Hartbrich and Dr. Friederike Bock from Oak Ridge National Laboratory for accepting me into the test beam and for taking care of me during my time in Geneva at CERN. A special thanks to Dr. Christine Nattrass, my advisor, for her unwavering support and guidance throughout the writing of this thesis and for her encouragement even before I joined the program. Additionally,I am deeply grateful to Maria Luiza, my partner, for her unwavering love, patience, and constant support. Finnally, I want to thank my friends, whose presence makes life infinitely more enjoyable.

"There are two possible outcomes: if the result confirms the hypothesis, then you've made a measurement. If the result is contrary to the hypothesis, then you've made a discovery."

Enrico Fermi, Nobel Prize laureate

Abstract

This thesis investigates the performance and calibration of the Longitudinally Segmented Forward Hadronic Calorimeter (LFHCAL) for the Electron-Ion Collider (EIC). The primary objective was to validate the design predictions through experimental data collected during a test beam campaign at CERN's T9 beamline. The LFHCAL module was subjected to Minimum Ionizing Particles (MIPs) using a 5 GeV muon beam to analyze its energy response, stability, and calibration. The study analyzed energy deposition using Landau-Gaussian fits to determine parameters like the Most Probable Value (MPV) and standard deviation. Results confirmed the detector's stable response and are a first step in the direction of a full working calorimeter.

Table of Contents

1 Electron-Ion collider and the ePIC collaboration **1**

1.1 Background and Motivation 1

1.1.1 Origin of Nucleon Spin 2

1.1.2 Nucleon's mass origin 4

1.2 LFHCAL Design 5

2 Test Beam **7**

2.1 Test Beam setup 7

3 Data Analysis and Calibrations **12**

3.1 Particles through matter 12

3.2 Muon Data Analysis 14

3.2.1 Landau-Gauss convolution 14

4 Results and Discussion **16**

4.1 MPV Distributions at Different Positions 18

4.2 Voltage variation study 21

4.2.1 Signal to Noise Ratio 21

5 Conclusions **24**

Bibliography **25**

A Energy Loss Calculations for 5 GeV Muons in the LFHCAL **26**

A.0.1 Stopping Power Interpolation 26

A.0.2 Energy Loss in the Iron Absorber Layer 27

A.1 Conversion constant 27

Vita **28**

Chapter 1

Electron-Ion collider and the ePIC collaboration

1.1 Background and Motivation

The Electron-Ion Collider (EIC) is proposed to be one of the main nuclear physics facilities in the United States. The Yellow Report [1] serves as the guiding document for the development of the EIC, laying out the specifications and requirements set forth by the science community to ensure the completion of the proposed scientific milestones.

The EIC aims to approach some of the biggest and most fundamental questions, such as the origins of nucleon mass, its spin, and the emergent properties of gluon systems. It will require a center-of-mass energy for $e + p$ collisions that ranges from $\sqrt{s} = 20\,\text{GeV}$ to $100\,\text{GeV}$. The center-of-mass energy, $\sqrt{s}$, is defined as:

1. If particle B is at rest in the lab frame ($E_B = m_B$ and E_A is the energy of the incident particle):
$$\sqrt{s} = \sqrt{m_A^2 + m_B^2 + 2m_B E_A}.$$

2. When A and B travel in opposite directions, the center-of-mass energy is:

$$\sqrt{s} = \sqrt{m_A^2 + m_B^2 + 2(E_A E_B + |\vec{p}_A||\vec{p}_B|)}.$$

For ultra-relativistic particles ($m_A, m_B \ll E_A, E_B$), this simplifies to:

$$\sqrt{s} \approx 2\sqrt{E_A E_B}.$$

In figure 1.1 we can see the top view of the EIC, highlighting its beam lines and detector position. A schematic drawing, shown in Figure 1.2, illustrates the full pseudo-rapidity coverage, ranging from $-4 < \eta < 4$, of the ePIC (Electron-Proton/Ion Collider) detector. The far backward region corresponds to the lepton endcap, while the far forward region corresponds to the hadron endcap, where the LFHCal will be installed alongside the ePIC's electromagnetic calorimeter (EEEMC). In the image, x is the momentum fraction of the struck parton in the parent proton and Q^2 refers to the square of the momentum transfer between the electron and proton. These are found by measuring the energies and angles of the final particles in the collisions, such as the scattered electron and the final hadronic state.

1.1.1 Origin of Nucleon Spin

Understanding the origin of nucleon spin, arising from the interactions of quarks and gluons and their respective spin and angular momentum, has been a problem in nuclear physics for decades[2]. The spin can be written in terms of its components

$$\frac{1}{2} = \frac{1}{2}\Delta\Sigma(\mu) + \Delta G(\mu) + L_{Q+G}(\mu), \tag{1.1}$$

in which $\Delta\Sigma, \Delta G(\mu)$ and L are the contributions from the quark plus antiquark spin, the gluon spin, and the parton angular momenta, respectively[1]. Since 1983 it has been known that $\Delta\Sigma$ can only account for a small part of the spin[3]. In the EIC,

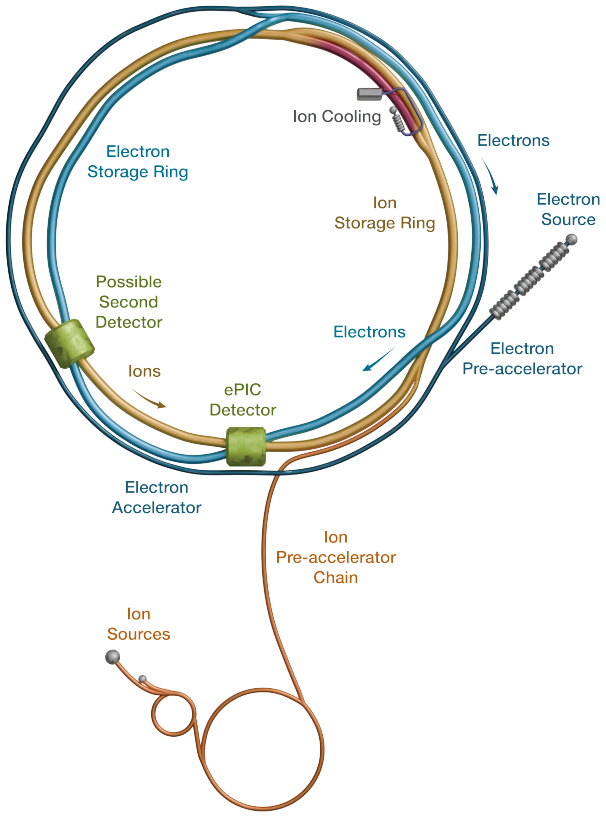


Figure 1.1: Top view of EIC's ring. [1]

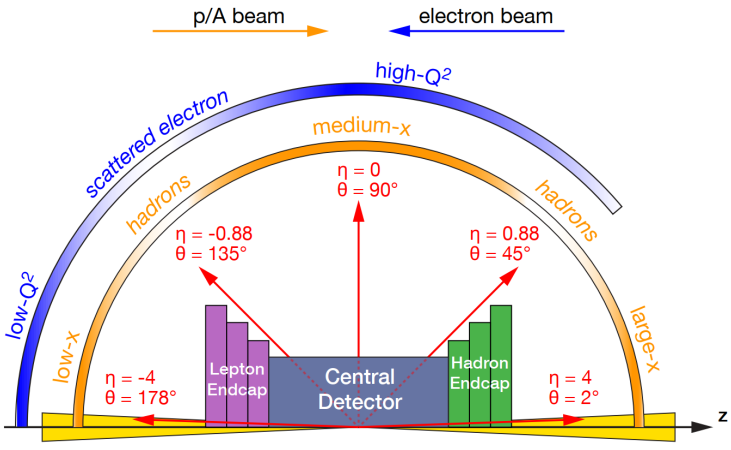


Figure 1.2: Schematic showing the different regions of the detector[1]

measurements of the parton helicity distribution are to be made at $x \leqq 0.05$, a resolution never before reached in any of the experiments at the Relativistic Heavy Ion Research Collider (RHIC)[4]. Precise measurements of deep inelastic scattering (DIS) events are crucial for understanding the origin of nucleon spin. For this, it will be essential that the EIC's electromagnetic calorimeters achieve high resolution in the far-backward region (small x). On the other end, in the far-forward region, reconstructing the hadronic states for high x will require the LFHCAL to have precise momentum and energy resolutions.

1.1.2 Nucleon's mass origin

Another know problem in nuclear physics is the origin of mass of protons and neutrons. If we were to sum their constituents, a trio of quarks, it would account for only about 1% of the total mass. The rest comes from strong interactions mediated by gluons. Lattice Quantum Chromodynamics (QCD) reproduces proton and neutron masses by computing dimensionless mass ratios normalized to the pion mass, demonstrating that the bulk of nucleon mass arises from interactions in the QCD vacuum [5].

At ePIC, quarkonia production, such as charmonia ($c\bar{c}$) and bottomonia ($b\bar{b}$), bound states of a heavy quark-antiquark pair, will be measured. Quarkonia are of particular interest because they are colorless, so all interactions are made through the exchange of gluons. In the lower x region of the hadron endcap, the energy required for quarkonia production is near the minimal threshold, making it an ideal process to probe the gluon distribution. At lower kinetic energies it is highly dependent on the gluon distribution in the nucleon, as well as highly sensitive to multigluon exchanges. These are subtle interactions and a high energy resolution detection system is essential.

1.2 LFHCAL Design

The Longitudinally Segmented Forward Hadronic Calorimeter (LFHCAL) is a central element of the forward detector system for the Electron-Ion Collider (EIC). Its role is to contain and measure the energy of hadrons as they interact with the detector's layers. The calorimeter is segmented in steel towers measuring 5cm x 5cm x 140cm. Each tower has 70 layers, alternating between 16mm of absorber and 4mm of plastic scintillator. The steel initiates the hadron shower while the scintillators detect the energy that is deposited by the particles that pass by.

The LFHCAL covers pseudorapidities in the $1.1 < \eta < 4$ range. This corresponds to small angles relative to the beamline, a region with high energy hadrons and jets, making the LFHCAL an essential tool for studying the hadronic structure and jet fragmentation processes. The physics program outlined by the Yellow Report[1] asks for high energy resolution. The LFHCAL is designed to have a resolution in the order of $\frac{33.2}{\sqrt{E}} \oplus 1.4\%$, in which the first term corresponds to the stochastic component and the second the constant. The stochastic part is inversely proportional to the square root of the energy, so it dominates at lower energies.

Table1.1 lists the specifications and expected resolution for the LFHCAL. The main objective of this thesis is to work on the performance assessment, ensuring readings are stable accross multiple operation variables and calibration of the calorimeter module by determining the energy deposition in ADC (Analog to Digital) counts of muons at a known energy of 5GeV.

Table 1.1: LFHCAL Parameters [6]

	LFHCAL
tower size	$5 \times 5 \times 140$ cm^3
material	Steel W/ Scintillator
d_{abs}	16 mm
d_{act}	4 mm
N_{layers}	70
X/X_O	65 - 72
R_M	21.11 cm
f_{sampl}	0.040
λ/λ_0	$\sim 7.6 - 8.2$
η acceptance	$1.1 < \eta < 4$
Energy resolution	$33.2/\sqrt{E} \oplus 1.4\%$

Chapter 2

Test Beam

2.1 Test Beam setup

The test beam was conducted on CERN's east area T9 beam line, as shown in figure 2.1, part of the Proton Syncroton (PS) ecosystem - built in 1959, with a 628m circumference and capable of accelerating protons up to 26GeV/c. Table 2.1 details some of the facility's parameters.

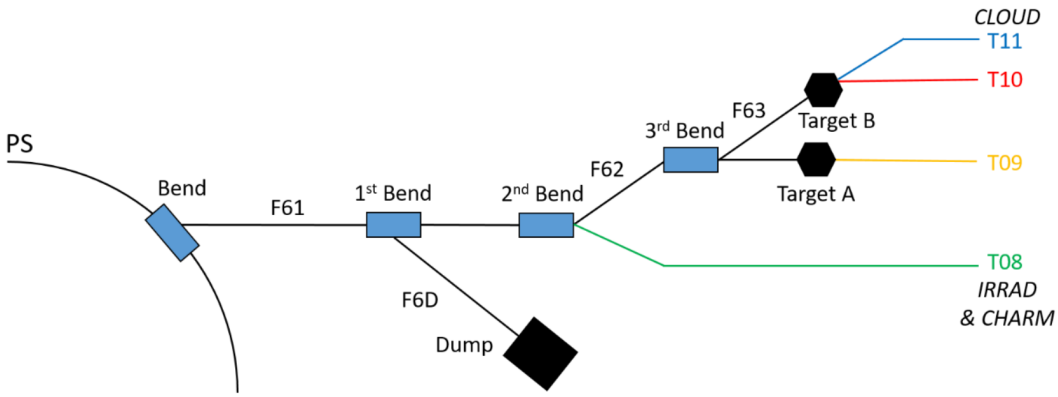


Figure 2.1: T9 beamline system [7]

The T9 area is ideal for test beam campaigns as it is able to produce a wide array of particles - such as protons, electrons, pions and muons - in the 1 GeV/c to 15GeV/c range. Protons from the PS are directed into a target, such as Target A, detailed in Table 2.2. Target A consists of multiple material heads: beryllium and aluminum for hadron beams, and tungsten for electron/positron beams. After interacting with the target, a set of quadrupole triplets focuses and shapes the beam - ensuring proper vertical and horizontal control of the beam profile. Further refinement is done down the line, where collimators refine the beam spread. Finally, bending magnets are used to select particles within the desired momentum.

Table 2.1: Beam Parameters for the T9 Beamline [7]

Parameter	**T09**
Length up to the last element [m]	50.2
Max. momentum [GeV/c]	15
Momentum resolution	0.7%
Max. momentum band	±15%
Horizontal magnification at final focus	0.86
Vertical magnification at final focus	0.9

Table 2.2: Target A Configuration in the T9 Beamline [8]

Head Number	**Material**	**Length (mm)**	**Purpose/Particle Production**
1	Beryllium (Be)	200	Hadron-rich production
2	Aluminum (Al)	100	Hadron-rich production
3	Aluminum (Al)	200	Additional hadron production
4	Tungsten (W)	3	Electron/positron-enriched beam
5	Air (empty)	-	Used for beam control

A muon filter is also available in the T9 beam line. It consists of a specialized system that can be configured using a movable stopper-dump. It is capable of filtering hadrons and electrons, ensuring a high purity muon beam. Alternatively, a pure muon beam can be achieved by closing the first collimator off-axis, which effectively filters out non-muon particles and leaves a similarly high-purity muon beam. Table 2.2 has more details about the target configurations in the T9 beamline.

The test beam setup consists of a pre-triggering external unit located before the calorimeter modules, which includes pairs of large and small scintillators (Fig. 2.3). These scintillators could be used one at a time, with the selection done manually (Fig. 2.2). A single calorimeter module was placed in a movable table on the (X, Y) axis called DESY table, which allows scanning of only half of the towers at a time when the table was placed at $(-5, 0)$ and the other half at $(5, 0)$ in centimeter units, a valuable asset used many times during data acquisition runs.

After leaving the beam pipe, particles travel a few meters, hit the external triggers, which tell the readout system to take data, then hit the first iron layer of the module. That is followed by the plastic scintillators that are then read by the Silicon Photomultipliers (SiPMs), present in every scintillating layer. This signal is then passed to eight different CAEN DT5202 SiPM readout units. CAEN's Janus v36 data acquisition system was used. The data from each run are then saved in text files containing information regarding board number, channel number, low and high gain readings, time stamp, trigger ID, and number of hits.



Figure 2.2: Changing scintillator type.

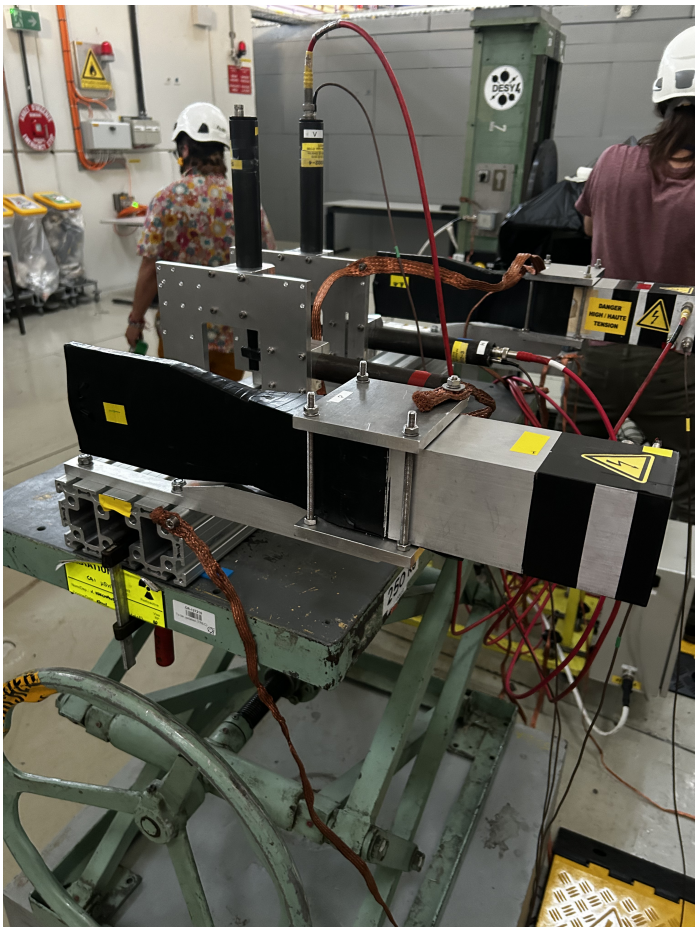


Figure 2.3: External scintillators used as a pre-trigger.

Chapter 3

Data Analysis and Calibrations

3.1 Particles through matter

When particles pass through a medium, they interact with the particles inside the material's structure and lose energy by ionization, radiative and scattering events. The mean rate of energy loss for a heavy particle is well modeled by the Bethe-Bloch equation, given by [9]

$$\left\langle \frac{dE}{dx} \right\rangle = Kz^2 \frac{Z}{A} \frac{1}{\beta^2} \left(\frac{1}{2} \ln \frac{2m_e c^2 \beta^2 \gamma^2 T_{\max}}{I^2} - \beta^2 - \frac{\delta}{2} \right), \tag{3.1}$$

in which K is a constant that normalizes the energy loss based on the properties of the material and z is the charge of the particle. Then Z and A are the atomic number and mass of the stopping material. By definition, $\beta = \frac{v}{c}$ and $\gamma = \sqrt{\frac{1}{1-\beta^2}}$. Finally, $T_{\max}$ is the highest transferable kinetic energy, I is the average ionization enegy for atoms in the material, and $\delta(\beta\gamma)$, dependent on both β and γ, is the correction to account for energy losses at high velocities due to medium polarization. In a simplified and practical approach, $\left\langle \frac{dE}{dx} \right\rangle$ is approximately a function of β alone and represents the mass stopping power of a given target. Figure 3.1 shows the energy deposition of muons in copper as a function of $\beta\gamma$.

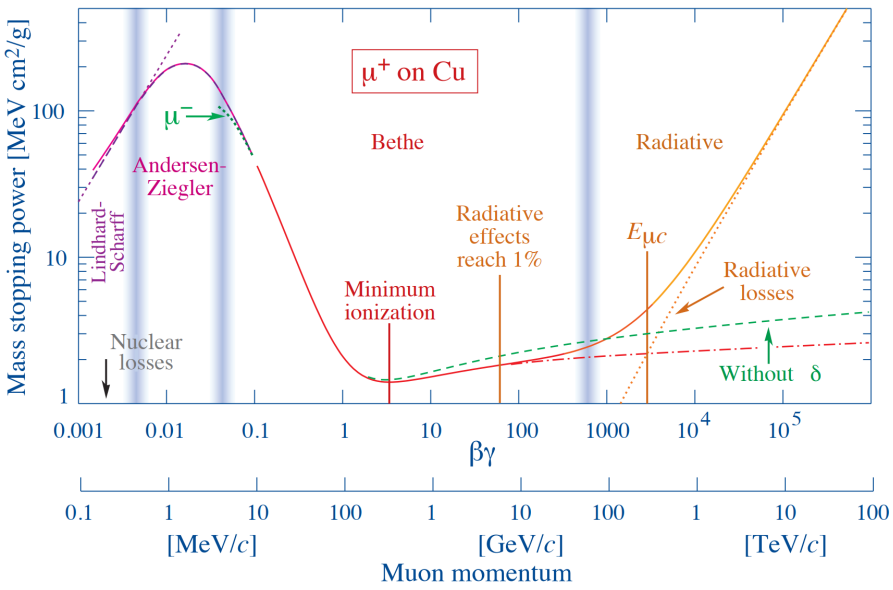


Figure 3.1: Energy deposition of positive muons in copper as a function of $\beta\gamma$ [9].

The particles that lose energy at the lower end of the distribution predicted by the Bethe-Bloch equation are know as Minimum Ionizing Particles (MIPs). Their energy loss is approximately constant and radiative losses are not as important.

Although robustly modeled, equation 3.1 is not reliable for finding the mean energy loss with a high level of confidence. That is because energy transfer events are skewed by rare and highly energetic particles that drive up the mean of the distribution. Instead, an alternate approach is to use the Landau-Vavilov distribution, given by [9]

$$\Delta_p = \xi \left[\ln \frac{2m_e c^2 \beta^2 \gamma^2}{I} + \ln \frac{\xi}{I} + j - \beta^2 - \delta(\beta\gamma) \right], \tag{3.2}$$

where $\xi = \frac{K}{2}\frac{Z}{A}\frac{z^2 x}{\beta^2}$ is dependent on the detector thickness x in gcm^{-2}. Here, Δ_p can be understood as the most probable value for the deposition energy of a given particle. The constant j is empirical. For high energy regimes, the radiative and ionization corrections are suppressed and energy losses reach a plateau,

$$\Delta_p \xrightarrow{\beta\gamma \gtrsim 100} \xi \left[\ln \frac{2m_e c^2 \xi}{(\hbar\omega_p)^2} + j \right]. \tag{3.3}$$

It is important to stress that the actual experimental distribution for the energy loss of particles passing through matter will be, therefore, long tailed as the rare high-energy events drive it away from the expected value calculated by the Bethe-Bloch formula. In an actual experimental setting, however, the Landau distribution alone also proves to be insufficient, as the process of measuring the particle's energies adds uncertainty and error to the signal due to limited detector resolution, electronic noise, and minor variations in the thickness of the traversed material, thus making it necessary the use of a Landau-Gaussian convolution that not only captures the intrinsic long-tailed energy distribution but also accounts for random variations introduced by the detection equipment.

3.2 Muon Data Analysis

The data used in this work were collected during the August 2024 LFHCAL test beam campaign. The LFHCAL is designed for energy measurements in the EPIC calorimeter system, and the test beam campaign aimed to validate its performance under various conditions.

Muons are used because they behave as Minimum Ionizing Particles (MIPs), meaning they lose the least amount of energy needed to produce a signal in the calorimeter. The distribution of energy deposited in the detector is analyzed by fitting it with a Landau-Gaussian (Langau) distribution. This fitting method provides a clear understanding of how muons lose energy in the calorimeter and allows us to find key values like the most probable value (MPV) of the energy lost in the calorimeter layers.

3.2.1 Landau-Gauss convolution

The Landau-Vavilov distribution is defined as

$$L(x; w, m) = \frac{1}{w} \exp\left(-\frac{1}{2}\left(\frac{x - m - e^{(x-m)}}{w}\right)\right)$$

in which x is the energy loss variable, m is the Most Probable Value (MPV) representing the peak of the distribution, and w is the width of the Landau distribution. It is a parametrized version of equation 3.2 and it is used because it is less computationally demanding than the original equation.

The Gaussian part of the convolution is given by

$$G(x;\mu,\sigma) = \frac{1}{\sqrt{2\pi}\sigma} \exp\left(-\frac{(x-\mu)^2}{2\sigma^2}\right)$$

in which, μ is the mean of the distribution, and σ is the standard deviation, representing the resolution of the detector.

To account for both the energy loss process and detector resolution, a convolution of the Landau and Gaussian distributions is used:

$$f_{\text{conv}}(x) = \int_{-\infty}^{\infty} L(y;w,m) \cdot G(x-y;\sigma)\, dy. \tag{3.4}$$

Here, $L(y;w,m)$ is the Landau distribution, and $G(x-y;\sigma)$ is the Gaussian distribution centered at x with standard deviation σ. This convolution combines the shape of the Landau distribution with the broadening effect of the Gaussian distribution, providing a realistic model to be used in this analysis.

Chapter 4

Results and Discussion

To evaluate the response of the full calorimeter module, the DESY table it was mounted on was moved within the range (-5,0) to (5,0). In this section, data from muon runs at 5GeV were analyzed. Each run contains about one hundred thousand events which were fitted using a Landau-Gauss convolution. Figure 4.1 illustrates the Landau-Gauss fit applied to the ADC count distribution of channel 16 on Board 2. The data points represent the measured ADC counts from the muon events, while the red curve represents the fitted Landau-Gauss function. The fit captures the asymmetric shape of the distribution, characteristic of energy deposition by muons. The Most Probable Value (MPV) is the most likely energy value for the Minimum Ionizing Particle.

To reduce noise, pedestal runs (data taken with no beam passing through the calorimeter module) were fitted using a normal Gaussian curve. The mean and standard deviation from the fit were then subtracted from the data across all boards and channels combinations. To further reduce noise and exclude channels with insufficient data, either due to the DESY table position or beam spread, ADC (Analog-to-Digital Converter) counts with fewer than five entries and boards with fewer than two thousand data points were omitted from the analysis.

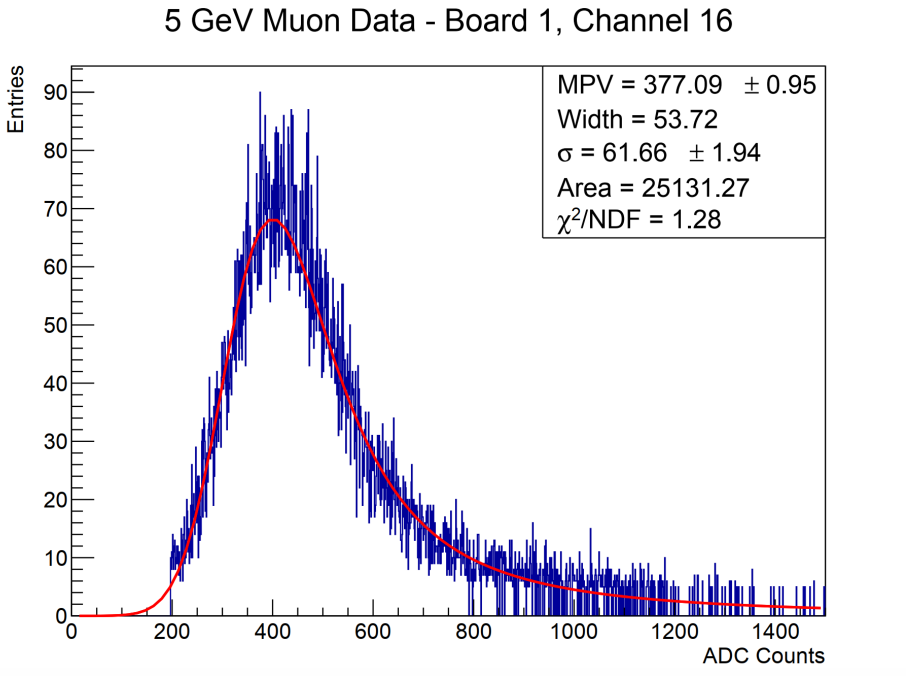


Figure 4.1: Landau-Gauss fit to the ADC count distribution for Channel 16 on Board 1 for a run taken at (-5,0) with an applied voltage of 45V. The data distribution represent the measured ADC counts, and the red curve is the fitted Landau-Gauss function.

4.1 MPV Distributions at Different Positions

To compare the module's response at different positions, namely with the DESY table at (-5,0) and (5,0), four data runs with around one hundred thousand events each were used. The high voltage applied to the SiPM boards was 45V for the first two and 42V for the others.

Figure 4.2 has the combined MPV distribution for runs 282 and 283, the ones with 45V applied to the boards while taking data. It has a mean of 320.8 ADC counts and a standard deviation of 61.79 ADC counts. Figure 4.3 shows the Most Probable Value distribution for the runs done at 42V and it shows a significantly reduced mean value, at 188.4 ADC counts with a standard deviation of 46.2 ADC counts.

To ensure accurate measurements, it is also important to closely examine the results from each board. Figures 4.4 and 4.5 show the MPV distributions in each board for runs 282 and 283. A consistent response can be observed in all boards, indicating that channels on both sides of each SiPM board are working similarly which is exactly the expected result of a working module. The same behavior is seen for the runs at 42V.

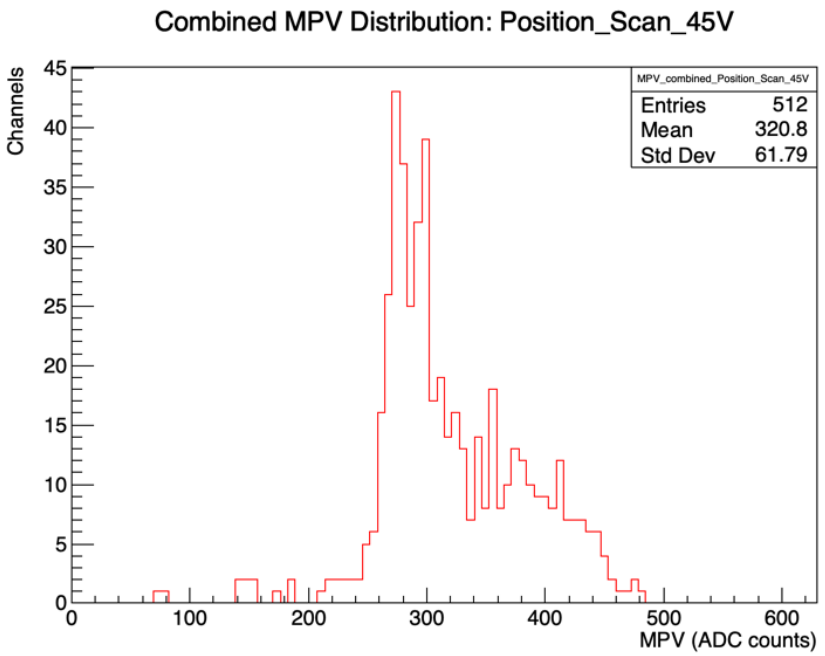


Figure 4.2: Most Probable Value (MPV) histogram of the combined runs 282 and 283 at 45V

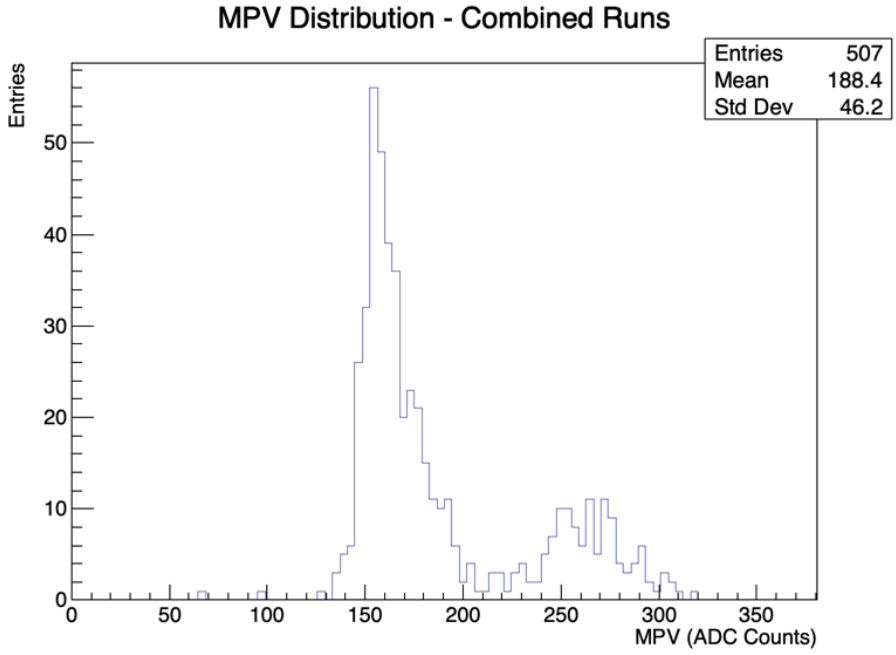


Figure 4.3: Most Probable Value (MPV) histogram of the combined runs 322 and 331 at 42V

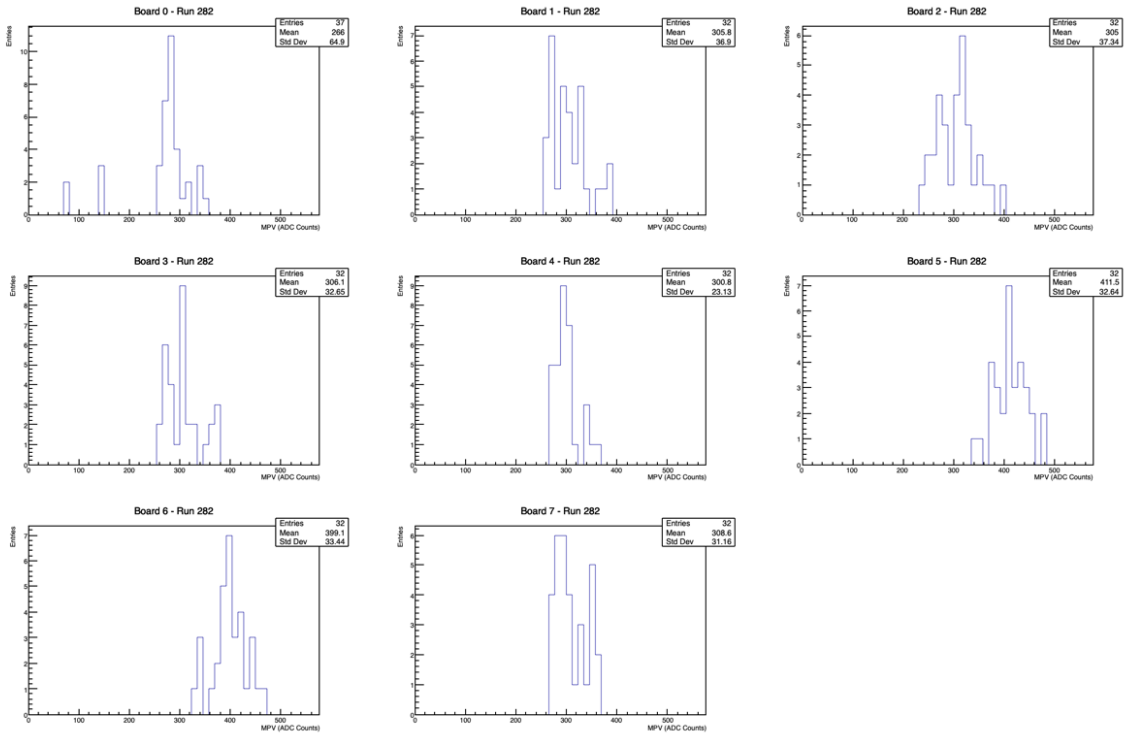


Figure 4.4: Most Probable Value distribution for all boards in Run 282

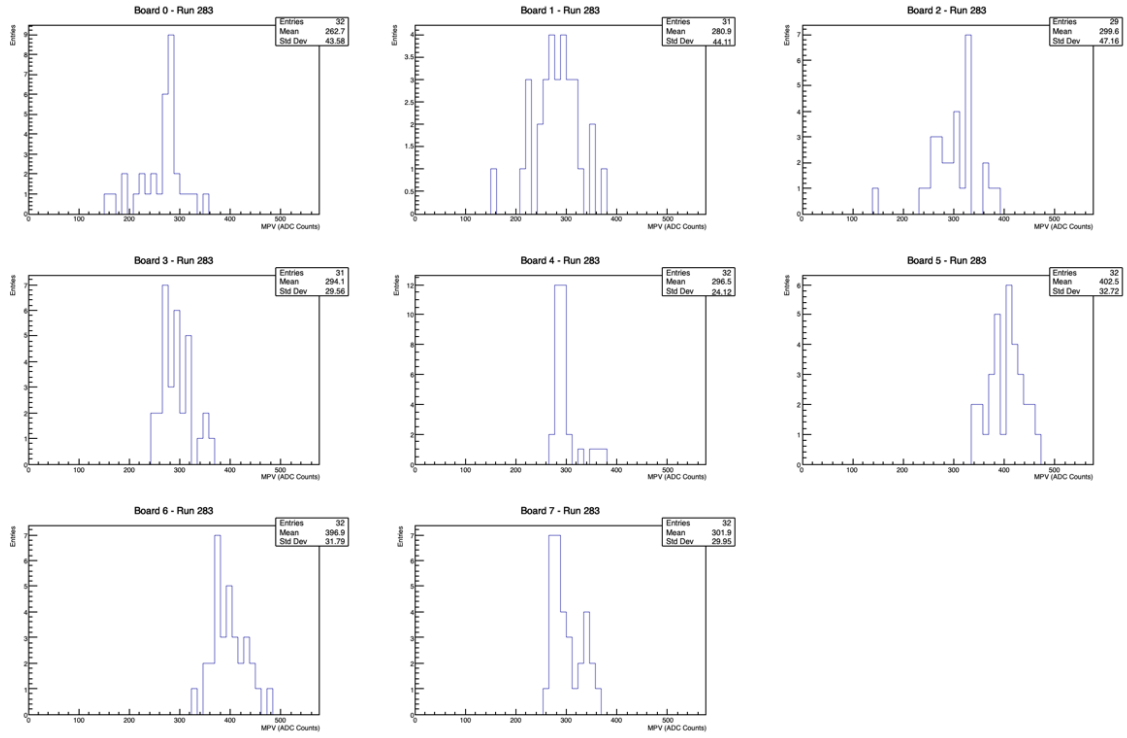


Figure 4.5: Most Probable Value distribution for all boards in Run 283

4.2 Voltage variation study

To understand the effect of the applied high-voltages in the data acquisition process, several data runs with V_a varying from 40V to 45V were taken. In this analysis runs with fifty thousand events each were used, taken at the (0,0) position. It can be easily seen on figure 4.6 that, on average, the most probable value of energy deposition recorded at the calorimeter module varies linearly with the applied voltage at the boards during the data taking runs.

4.2.1 Signal to Noise Ratio

By taking a closer look at the behavior of the standard deviations of the pedestal distributions, plotted in figure 4.7, the impact of noise in the readings can be better understood. In practice, noise grows quadratically with the applied voltage, thus an optimal operation voltage can be found such that noise strength is maximized while noise is reduced.

The Signal-to-Noise ratio (SNR) is simply defined as

$$SNR = \frac{MPV}{\sigma_{pedestal}}, \tag{4.1}$$

and it is a metric of signal quality. Values above 1 indicate that signal can be distinguished from background noise. Figure 4.8 suggests the existence of a maxima somewhere between 42V and 44V.

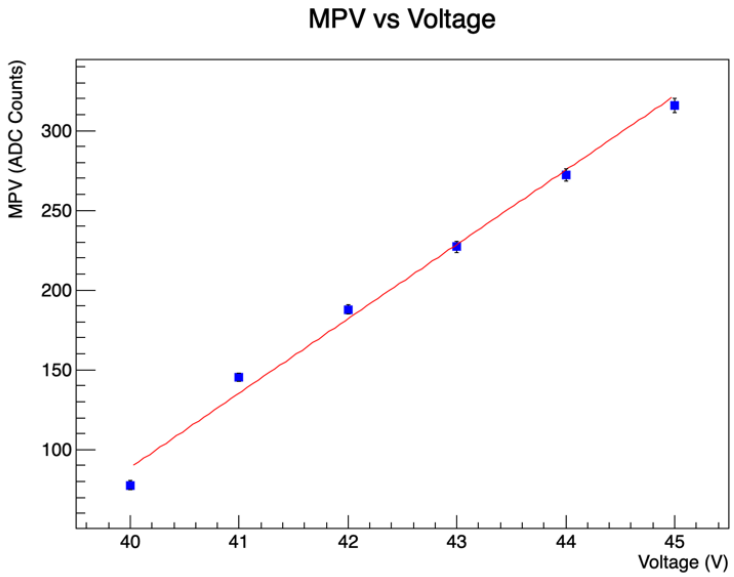


Figure 4.6: Average of Most Probable Value in each run as a function of the applied voltage.

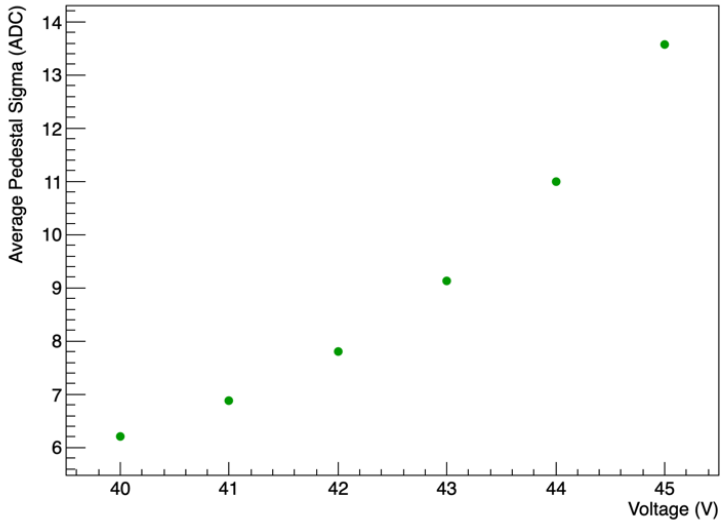


Figure 4.7: Standard deviation of the pedestal signal as a function of the applied voltage.

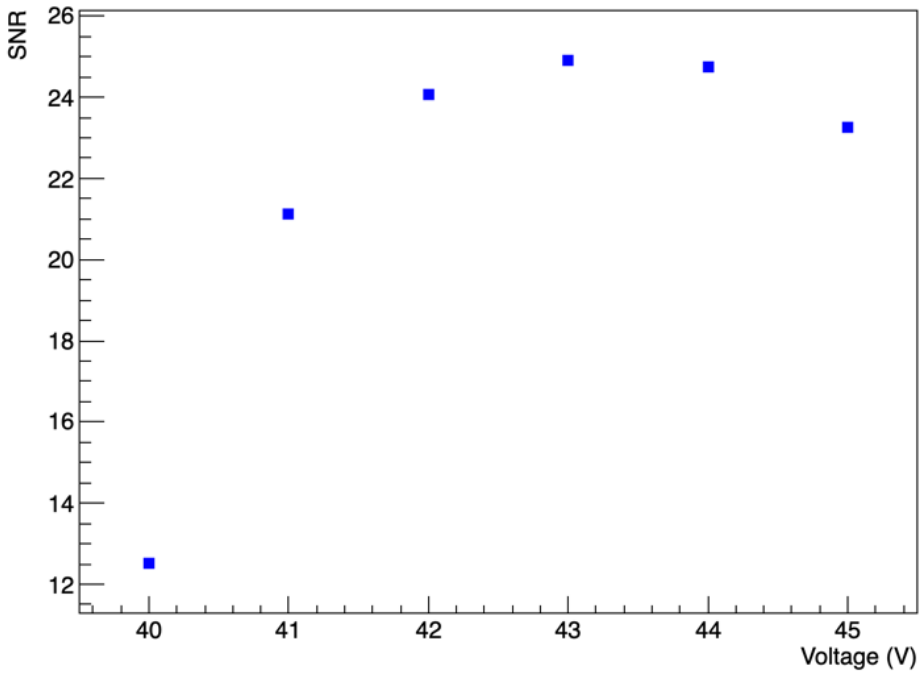


Figure 4.8: Signal-to-Noise ratio as a function of the applied voltage

Chapter 5

Conclusions

The work presented in this thesis highlights the initial testing and validation of the Longitudinally Segmented Forward Hadronic Calorimeter (LFHCal) module at the T9 Beamline of CERN. Contributions included the physical assembly of the module and its electronics, data acquisition, and analysis using Landau-Gaussian fits to extract key performance metrics such as the MPV and SNR. These results confirm the module's stability and alignment with design expectations for Minimum Ionizing Particle detection. The LFHCal is now ready to advance into the next phase of testing, which involves multiple modules and broader-scale analyses. Comprehensive studies of the LFHCal's performance in varied conditions and its full integration into the ePIC detector will be conducted by the collaboration, ensuring its readiness for deployment at the Electron-Ion Collider.

Bibliography

[1]R Abdul Khalek et al., "Science Requirements and Detector Concepts for the Electron-Ion Collider: EIC Yellow Report", Nuclear Physics A **1026**, 122447 (2022).

[2]X. Ji, F. Yuan, and Y. Zhao, "What we know and what we don't know about the proton spin after 30 years", Nature Reviews Physics **3**, 27–38 (2021).

[3]J. J. Aubert et al., "The ratio of the nucleon structure functions F2N for iron and deuterium", Physics Letters B **123**, 275–278 (1983).

[4]E.-C. Aschenauer and others, "The RHIC SPIN Program: Achievements and Future Opportunities", (2015).

[5]S Dürr et al., "Ab Initio Determination of Light Hadron Masses", Science **322**, 1224–1227 (2008).

[6]J. K. Adkins et al., "Design of the ECCE Detector for the Electron Ion Collider", (2022).

[7]J. Bernhard et al., "CERN Proton Synchrotron East Area Facility Upgrades and renovation during Long Shutdown 2 Editors", 10.23731/CYRM-2021-004.

[8]*Information about the T9 beam line and experimental facilities*, tech. rep. ().

[9]S Navas et al., "Review of Particle Physics", Physical review. D/Physical review. D. **110**, 10.1103/physrevd.110.030001 (2024).

Appendix A

Energy Loss Calculations for 5 GeV Muons in the LFHCAL

A.0.1 Stopping Power Interpolation

To determine the muon stopping power at 5 GeV, a linear interpolation is performed between the tabled values at 4 GeV and 8 GeV [9]. The stopping power ($\frac{dE}{dx}$) in iron at these energies is given by

$$\left(\frac{dE}{dx}\right)_{4\,\mathrm{GeV}} = 1.816\,\mathrm{MeV\,cm^2 g^{-1}}, \tag{A.1}$$

$$\left(\frac{dE}{dx}\right)_{8\,\mathrm{GeV}} = 1.935\,\mathrm{MeV\,cm^2 g^{-1}}. \tag{A.2}$$

The interpolation is done in the following fashion

$$\begin{aligned}\left(\frac{dE}{dx}\right)_{5\,\mathrm{GeV}} &= \left(\frac{dE}{dx}\right)_{4\,\mathrm{GeV}} + \left(\frac{\left(\frac{dE}{dx}\right)_{8\,\mathrm{GeV}} - \left(\frac{dE}{dx}\right)_{4\,\mathrm{GeV}}}{8\,\mathrm{GeV} - 4\,\mathrm{GeV}}\right) \times (5\,\mathrm{GeV} - 4\,\mathrm{GeV}) \\ &= 1.816\,\mathrm{MeV\,cm^2 g^{-1}} + \left(\frac{1.935\,\mathrm{MeV\,cm^2 g^{-1}} - 1.816\,\mathrm{MeV\,cm^2 g^{-1}}}{4\,\mathrm{GeV}}\right) \times 1\,\mathrm{GeV} \\ &= 1.816\,\mathrm{MeV\,cm^2 g^{-1}} + 0.02975\,\mathrm{MeV\,cm^2 g^{-1}} \\ &= 1.84575\,\mathrm{MeV\,cm^2 g^{-1}}. \end{aligned} \tag{A.3}$$

Thus, the stopping power of 5 GeV muons in iron is approximately $1.846\,\mathrm{MeV\,cm^2 g^{-1}}$.

A.0.2 Energy Loss in the Iron Absorber Layer

Using the interpolated stopping power, the energy loss in the iron absorber layer (ΔE_{Fe}) can be calculated. The density of iron (ρ_{Fe}) is $7.874\,\mathrm{g\,cm^{-3}}$, and the thickness of the absorber layer (d_{abs}) is 1.6 cm. The energy loss is given by

$$\Delta E_{\mathrm{Fe}} = \left(\frac{dE}{dx}\right)_{\mathrm{Fe}} \times \rho_{\mathrm{Fe}} \times d_{\mathrm{abs}}. \tag{A.4}$$

Substituting the values:

$$\begin{aligned} \Delta E_{\mathrm{Fe}} &= 1.846\,\mathrm{MeV\,cm^2 g^{-1}} \times 7.874\,\mathrm{g\,cm^{-3}} \times 1.6\,\mathrm{cm} \\ &= 1.846 \times 7.874 \times 1.6\,\mathrm{MeV} \\ &= 23.28\,\mathrm{MeV}. \end{aligned} \tag{A.5}$$

Therefore, a 5 GeV muon loses approximately 23.28 MeV of energy per iron absorber layer.

A.1 Conversion constant

Since the sampling factor in the LFHCAL is $f_{sampl} = 0.040$, then the measured energy in each layer of the calorimeter is only 0.9312 MeV. This means a conversion constant can be defined by assuming that each measured MIP in the read signal is equivalent to this exact amount of energy, such that a channel-specific conversion constant can then be calculated.

Vita

Thibor R. R. Bernardon was born on August 21, 1997, in Erechim, Brazil, the birthplace of his childhood football (not soccer) idol. He completed his Bachelor of Science in Physics at the State University of Maringá, Brazil, in 2021 and pursued a Master of Science in Physics at the University of Tennessee, Knoxville, from 2022 to 2024.

During his master's studies, Thibor participated in the testing of Longitudinally Segmented Forward Hadronic Calorimeter (LFHCal) modules for the ePIC detector at CERN. He contributed to data acquisition and detector performance analysis during a test beam campaign at CERN's Proton Synchrotron Complex. In addition to his research, Thibor served as a Graduate Teaching Assistant, assisting in undergraduate physics laboratories and supporting students' understanding of physics concepts. Outside of academia, Thibor enjoys geopolitics, cooking, and supporting his favorite football team, Sport Clube Internacional.